ELSEVIER

Journal of Non-Crystalline Solids 180 (1994) 40–50

JOURNAL OF NON-CRYSTALLINE SOLIDS

Structural study of Rb and (Rb,Ag) germanate glasses by EXAFS and XPS

W.C. Huang [a], H. Jain [a,*], M.A. Marcus [b]

[a] *Department of Materials Science and Engineering, Lehigh University, Bethlehem, PA 18015, USA*
[b] *AT&T Bell Laboratories, Murray Hill, NJ 07974, USA*

Received 20 December 1993; revised manuscript received 7 June 1994

Abstract

The interatomic distance, R, coordination number, CN, and degree of disorder, $\Delta\sigma^2$, around the mobile (Rb,Ag) as well as the network-forming (Ge) cations are obtained using EXAFS (extended X-ray absorption fine structure) of $x\mathrm{Rb_2O}\cdot(1-x)\mathrm{GeO_2}$ and mixed rubidium–silver germanate $0.2[y\mathrm{Ag}\cdot(1-y)\mathrm{Rb}]_2\mathrm{O}\cdot 0.8\mathrm{GeO_2}$ glasses with $x = 0.01$, 0.02, 0.05, 0.10, 0.15, 0.20, 0.30, 0.40 and $y = 0$, 0.25, 0.50, 0.75, 1.00. The non-bridging oxygen (NBO) and bridging oxygen (BO) concentrations are determined by X-ray photoelectron spectroscopy. With the addition of $\mathrm{Rb_2O}$, both $\mathrm{GeO_6}$ and NBOs are produced for all $x \le 0.2$. For $x > 0.2$, NBOs continue to increase at the expense of $\mathrm{GeO_6}$ units. A comparison of molar volume with various bond lengths indicates the presence of an 'unoccupied volume' which may vary with composition without affecting various interatomic distances. Replacement of Rb by Ag in mixed germanate glasses has the same effect on $R_{\mathrm{Rb-O}}$ and $\Delta\sigma^2_{\mathrm{Rb-O}}$ as the reduction of Rb content in single Rb germanate glasses. The $R_{\mathrm{Ag-O}}$ and $\Delta\sigma^2_{\mathrm{Ag-O}}$ show a trend opposite to that of the bond around Rb when Ag and Rb replace each other.

1. Introduction

The germanate glasses are potential materials for low-loss optical applications such as optical fibers and IR transmitting windows [1]. Their use as the medium of Raman fiber-optical amplifiers appears promising after the discovery of high Raman scattering [2,3]. It has been known for a long time that when an alkali oxide is added germanate glasses, by contrast with silicate glasses, show a maximum or minimum in physical properties such as density and refractive index [4]. More recently a minimum in ionic conductivity of alkali germanate glasses as a function of alkali oxide concentration was reported by Mundy and Jin [5]. This phenomenon is often referred as the 'germanate anomaly' in analogy to the well known 'boron anomaly' in borates [6,7]. It is popularly explained [4] by the formation of $\mathrm{GeO_6}$ octahedra with the addition of 0–15 mol% $\mathrm{M_2O}$ (M = alkali) leading to densification, followed by the formation of both $\mathrm{GeO_4}$ tetrahedra and non-bridging oxygens above 15 mol% $\mathrm{M_2O}$, resulting in a loosening of the network structure. The explanation appears reasonable because in silicate glasses the addition of alkali oxide merely loosens the glass structure by forming non-bridging oxygens, while maintaining the tetrahedral units instead of forming octahedral structural units [8–10]. However, one-to-one correspondence has not been established between the

* Corresponding author. Tel: +1-610 758 4217. Telefax: +1-610 758 4244.

SSDI 0022-3093(94)00438-2

variations of properties and structure of germanates. In fact, Henderson and Fleet [11] insist from their micro-Raman spectroscopy of sodium germanate glasses that the anomalous behavior does not result from $GeO_4 \rightarrow GeO_6$ conversion but from the formation of three-membered rings of GeO_4 tetrahedra. Clearly, there is continuing controversy on how the structure of germanate glasses changes by the addition of alkali oxide.

About a decade ago, Greaves el al. [12] conducted pioneering EXAFS experiments on a few silicate glasses and determined the local structure around sodium and silicon. They found that the width of the first-neighbor peak, i.e., the Na–O distance distribution, was no more than could be expected from thermal motion. Therefore, they postulated that the alkali ions in silicate glasses were not really distributed randomly as expected from Zachariasen's continuous random network (CRN) model [8]. These ions were considered to have a rather well defined environment to the extent that the structure of glass may be considered to consist of regions rich in mobile ions separated by regions devoid of such ions [13]. This hypothesis is the basis of their proposed modified random network (MRN) model of glass structure vis-à-vis the CRN model. If this new MRN model of glass is generally true, it has very far-reaching implications for our understanding of various properties, especially those dependent on the distribution and movement of alkali ions [14]. Computer simulations and molecular dynamic calculations of the structure of silicate glass have also indicated segregation of alkali ions, which is consistent with the MRN structure [15–17]. However, there is no report of direct microscopic observation of microheterogeneity on the scale postulated in the MRN structure. Also, it is not clear how universal such microsegregation is, if it does exist.

So, the present work is motivated by the need to further establish the structure of alkali germanates and to verify the applicability of MRN model to a glass system which is significantly different from alkali silicates. We have selected the $x\mathrm{Rb_2O} \cdot (1-x)\mathrm{GeO_2}$ glass series, for which one can conveniently determine local structure around the mobile Rb as well as network-forming Ge by using EXAFS. By contrast with alkali silicate systems, the alkali germanates do not phase-separate readily and, therefore, one would expect them to show less, if any, microheterogeneity. In other words, we expect Rb to be relatively randomly distributed in germanates compared with Rb in silicates. EXAFS is expected to reveal this difference in structure disorder. Further, we use X-ray photoelectron spectroscopy (XPS) to determine the relative fractions of bridging oxygen (BO) and non-bridging oxygen (NBO) [10,18]. The BO/NBO ratio is then used to determine the ratio of sixfold to fourfold Ge coordination. Thus, by combining the results of EXAFS and XPS, a more detailed structure of germanate glass is revealed.

The mixed (alkali) mobile ion (MMI) effect represents dramatic non-linear changes in ion transport when two mobile ions are mixed, but physical properties such as density, molar volume, thermal expansion, etc., vary nearly linearly with chemical composition [19]. Therefore, it is natural to ask whether the short-range local structure, by contrast with physical properties, has any significance for the MMI effect as indicated by a recent IR study [20]. Accordingly, we have included $0.2(\mathrm{Rb,Ag})_2\mathrm{O} \cdot 0.8\mathrm{GeO_2}$ glass series in this investigation and determined local structure around the two cations, Ag and Rb, as well as Ge.

2. Experimental

2.1. Glass preparation

Eleven glass compositions were prepared to form two glass series: $x\mathrm{Rb_2O} \cdot (1-x)\mathrm{GeO_2}$ with $x =$ 0.01, 0.02, 0.05, 0.10, 0.15, 0.20, 0.30, 0.40 and $0.2[y\mathrm{Ag} \cdot (1-y)\mathrm{Rb}]_2\mathrm{O} \cdot 0.8\mathrm{GeO_2}$ with $y = 0$, 0.25, 0.50, 0.75, 1.00. The first series is used to examine the effect of alkali concentration on germanate structure; the second series is prepared to investigate MMI effect with the total mobile ion concentration fixed while varying the ratio of the two mobile ions. The samples were prepared by the melt-quench method. Appropriate amounts of puratronic grade [1] GeO_2 (99.999%) and analytical grade [1] Rb_2CO_3 (99.8%), Ag_2O (99 + %) powders were thoroughly

[1] Johnson Matthey, Ward Hill, MA 01835, USA.

mixed (for ~ 10 h) and preheated at 900 to 1000°C for 1 h and then melted in a platinum crucible. Because of the reactivity of silver with platinum, an alumina crucible was used when glasses contained silver. The liquid was equilibrated for about 1 h at a temperature between 1200 and 1450°C depending on the composition and viscosity. Homogenized bubble-free liquid was cast in a stainless steel mold and then the glass was annealed at ~ 450°C for ~ $\frac{1}{2}$ h to remove internal stress before furnace cooling to room temperature. The resulting samples were cut into thin plates with dimensions ~ 1 $cm^2 \times 0.5$ mm for XPS and ground into fine powders for EXAFS spectroscopy. Some silver precipitated out of the Ag_2O-containing liquids and settled at the bottom of crucible. So the actual Ag concentration in glass is less than the batch composition [21]. However, this loss of silver does not qualitatively change the observation of mixed alkali effect in the present samples [22].

2.2. EXAFS experiment

To eliminate self-absorption effects, it was necessary to prepare thin glass samples for which the change in optical depth on crossing the absorption edge was ≤ 0.1 [23]. For this reason, the glass was powdered to ~ 5 μm particle size by grinding in polystyrene solution with a mortar and pestle. The powder was mixed with ~ 200 ml polystyrene–toluene solution in a 250 ml beaker containing a closely fitting filter paper at its bottom. Next the solution was left undisturbed until the powder settled onto the filter paper and the supernatant solution became clear (about 6 h later). Then the clear supernatant solution was pipetted out and the powder on the filter paper was dried and protected with an adhesive tape.

The K-edge EXAFS spectra of Ge (11.10 keV), Rb (15.20 keV) and Ag (25.52 keV) in both Rb germanate and Rb–Ag germanate glasses were recorded on the X6B beamline equipped with a Si (220) monochromator, at National Synchrotron Light Source, Brookhaven National Laboratory, Upton, NY, USA (for details of EXAFS with synchrotron radiation, see Ref. [24]). The transmitted X-ray intensities were measured at room temperature with a Lytle detector or plastic scintillator, while the fluorescence X-ray intensity was measured with an ion chamber [25]. Data analysis for background subtraction, normalization and Fourier transformation of raw spectra was carried out using programs developed at AT&T [26] and the SEXIE program of Rupp et al. [27]. GeO_2 and Ag_2O were used as model compounds for the determination of standard parameters, namely, interatomic distance, R_{M-O}, coordination number, CN, and Debye–Waller factor ($\Delta\sigma^2$, the mean square variation in interatomic distance). Since the Rb–O distance distributions in Rb oxide, nitrate, carbonate and acetate compounds are all broad and complex, we used the FEFF program of Rehr et al. [28] to model the Rb–O and Rb–Ge amplitudes and phase shifts. In some of the silver-containing samples there was an indication of Ag precipitation. However, results for only those samples are included in this paper for which there was negligible contribution from Ag–Ag EXAFS.

2.3. XPS experiment

The XPS measurements were carried out on a spectrometer (Scienta ESCA-300) with Al Kα X-ray source (1486.67 eV). To avoid surface contamination, the sample was fractured in situ in a vacuum better than 3.7×10^{-9} Torr. The photoelectrons were generated from the fracture surface of area about 10×1 mm^2. The surface was flooded with 4 to 10 eV electrons for minimizing charging. The X-ray spot size was about 1.6×0.3 mm^2. The step size (referring to the internal kinetic energy of photoelectron) in the analyzer was 0.1 eV and the energy resolution was 0.4 eV, as determined at the Fermi edge of Ag metal. The photoelectron energy was determined with a hemispherical analyzer. Data analysis was carried out with ESCA-300 software package using a least-square Gaussian fit and Shirley background substraction [29]. The relative XPS peak position, full width at half maximum (FWHM) and intensity (peak area) ratio were determined with this program.

3. Results

3.1. EXAFS spectra

EXAFS spectra have been obtained around Ge, Rb and Ag K-absorption edges in both the single

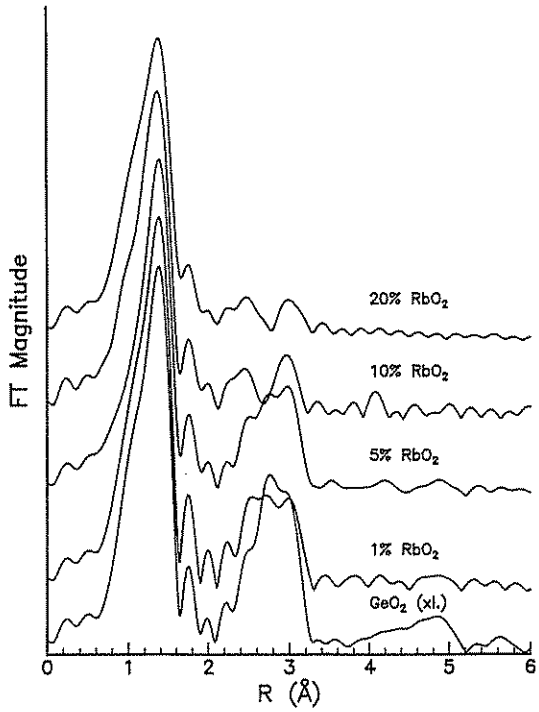

Fig. 1. Fourier magnitudes of $k^2\chi(k)$ extracted from EXAFS spectra for Ge K-edge in $x\mathrm{Rb_2O}\cdot(1-x)\mathrm{GeO_2}$ glasses.

mobile ion Rb germanate and mixed mobile ion Rb–Ag germanate glass series. The normalized EXAFS, $\chi(k)$, was multiplied by k^2 to amplify the magnitude of EXAFS in the high-k region, where k is the X-ray wave vector. The Fourier magnitudes of $k^2\chi(k)$ for the Ge K-edge in $x\mathrm{Rb_2O}\cdot(1-x)\mathrm{GeO_2}$ series for different values of x (up to 20 mol%) are shown in Fig. 1. After applying phase shift correction, we obtain the desired structural parameters. The basic principle of EXAFS and standard procedure for EXAFS data analysis and processing are given in Refs. [30–32]. The spectrum for the model compound, GeO_2, is also shown in Fig. 1. In this figure, we see a well defined peak corresponding to the first shell neighbor, which is assigned to Ge–O.

From EXAFS spectra in Fig. 1, the bond distance, CN and structural disorder around the first neighbor have been determined with respect to GeO_2 standard. Statistical analysis of the data indicates that the present results are relatively more accurate for Ge EXAFS than for Rb or Ag EXAFS. The estimated uncertainty for Ge–O distance is ± 0.01 Å but for the Rb–O distance it is $\leq \pm 0.03$ Å. In general, the uncertainty in CN is high and is typically 30%. The

Table 1
Structural parameters extracted from Ge (first shell) EXAFS: Ge–O bond distance, coordination number and disorder (Debye–Waller factor) around Ge atom in rubidium germanate and rubidium–silver germanate glasses

$\%Ag_2O$	$\%Rb_2O$	R_{Ge-O} (Å)	CN_{Ge-O}	$\Delta\sigma^2_{Ge-O}$ ($\times 10^{-4}$ Å^2)
$xRb_2O\cdot(1-x)GeO_2$				
0	2	1.74(0)	4.8	7
0	5	1.74(1)	4.4	8
0	10	1.74(6)	4.8	23
0	15	1.76(1)	4.0	12
0	20	1.75(5)	4.2	16
$0.2[yAg\cdot(1-y)Rb]_2O\cdot 0.8GeO_2$				
0	20	1.75(5)	4.2	16
5	15	1.75(2)	4.2	14
10	10	1.75(0)	4.0	19
15	5	1.74(4)	4.0	7
20	0	1.74(5)	4.0	6

first shell information corresponding to Ge–O is listed in Table 1, which also gives the results for the Rb–Ag mixed mobile ion series. There is an increase of Ge–O bond distance with increasing Rb_2O mol% as shown in Fig. 2, in which the bond distances of Ge–O in GeO_4 quartz-type and GeO_6 rutile-type structures are also drawn for reference to reveal the existence of GeO_6 structural units.

Parallel analysis of Rb EXAFS gives the Rb–O distance, CN and disorder around Rb as listed in

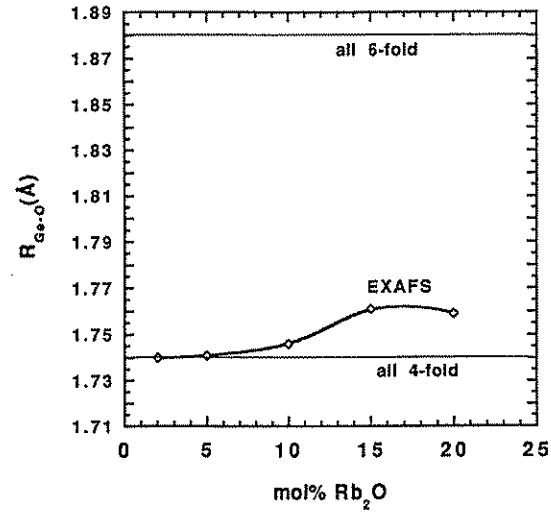

Fig. 2. Ge–O bond distance, R_{Ge-O}, as a function of mol% Rb_2O. The Ge–O bond distances in quartz-type (fourfold) and rutile-type (sixfold) crystalline GeO_2 are shown for comparison.

Table 2
Structural parameters extracted from Rb (first shell) EXAFS: Rb–O bond distance, coordination number and disorder (Debye–Waller factor) around Rb atom in rubidium germanate and rubidium–silver germanate glasses

$\%Ag_2O$	$\%Rb_2O$	R_{Rb-O} (Å)	CN_{Rb-O}	$\Delta\sigma^2_{Rb-O}$ ($\times 10^{-4}$ Å^2)
$xRb_2O\cdot(1-x)GeO_2$				
0	1	2.81(2)	5.6	220
0	2	2.82(6)	6.1	234
0	5	2.82(1)	5.5	185
0	10	2.82(4)	7.9	178
0	15	2.76(6)	5.6	119
0	20	2.73(5)	5.2	129
$0.2[yAg\cdot(1-y)Rb]_2O\cdot 0.8GeO_2$				
0	20	2.73(5)	5.2	129
5	15	2.78(3)	4.4	103
10	10	2.78(9)	6.5	162
15	5	2.80(9)	6.2	195
20	0			

Table 3
Structural parameters extracted from Rb (second shell) EXAFS: Rb–Ge bond distance, coordination number and disorder (Debye–Waller factor) around Rb atom in rubidium germanate and rubidium–silver germanate glasses

$\%Ag_2O$	$\%Rb_2O$	R_{Rb-Ge} (Å)	CN_{Rb-Ge}	$\Delta\sigma^2_{Rb-Ge}$ ($\times 10^{-4}$ Å^2)
$xRb_2O\cdot(1-x)GeO_2$				
0	1	3.71	6.0	186
0	2	3.72	6.0	183
0	5	3.72	6.5	209
0	10	3.72	4.1	130
0	15	3.68	8.3	224
0	20	3.68	7.2	228
$0.2[yAg\cdot(1-y)Rb]_2O\cdot 0.8GeO_2$				
0	20	3.68	7.2	228
5	15	3.70	5.6	193
10	10	3.68	7.6	199
15	5	3.71	6.3	167
20	0			

Table 2. The Rb–O distance remains constant within experimental error for $Rb_2O \leq 10$ mol% and then begins to decrease with the further addition of Rb_2O (≥ 15 mol%). In Rb EXAFS we also observe the second shell of atoms around Rb and obtain the corresponding parameters for the Rb–Ge bond (Table 3). Finally, the local structure around Ag was determined in the mixed mobile ion series and the results for the Ag–O bond are given in Table 4. The molar volume of Rb germanate glasses was also measured and the value is plotted in Fig. 3 together with the Rb–O and Ge–O bond distances. Note that the molar volume clearly shows a minimum at Rb_2O concentration between 5 and 10 mol%, but the Rb–O and Ge–O distances monotonically decrease and increase, respectively, with increasing Rb_2O, the relative variation of molar volume being much larger.

3.2. XPS spectra

The O 1s X-ray photoelectron spectra of the Rb germanate glasses consist of a predominant peak at $E_0 \sim 533$ eV and a smaller component at ~ 2 eV lower binding energy. Fig. 4 shows these spectra with E_0 as the reference energy. Fig. 5 shows the deconvolution of the O 1s spectrum into two peaks for $0.3Rb_2O\cdot 0.7GeO_2$ glass using the ESCA-300 software package. The corresponding peak values for each O 1s component are listed in Table 5. Note that, although the absolute values of the O 1s binding energy in Table 5 may have uncertainty > 0.1 eV due to incomplete neutralization of surface charge, the relative values are expected to be accurate to better than ± 0.1 eV. The intensity of the lower binding energy component increases with increasing Rb_2O concentration. It is attributed to NBOs in germanate glasses and the higher binding energy component is attributed to BOs [18]. Here a shift of the photoelectron peak toward lower binding energies corresponds to an increase in electron density on the relevant atom. That is, the difference in electron

Table 4
Structural parameters extracted from Ag (first shell) EXAFS: Ag–O bond distance, coordination number and disorder (Debye–Waller factor) around Ag atom in rubidium–silver germanate glasses

$\%Ag_2O$	$\%Rb_2O$	R_{Ag-O} (Å)	CN_{Ag-O}	$\Delta\sigma^2_{Ag-O}$ ($\times 10^{-4}$ Å^2)
$0.2[yAg\cdot(1-y)Rb]_2O\cdot 0.8GeO_2$				
0	20			
5	15	2.09(6)	1.2	82
10	10	2.17(4)	1.3	144
15	5	2.25(0)	2.0	245
20	0	2.24(5)	2.5	273

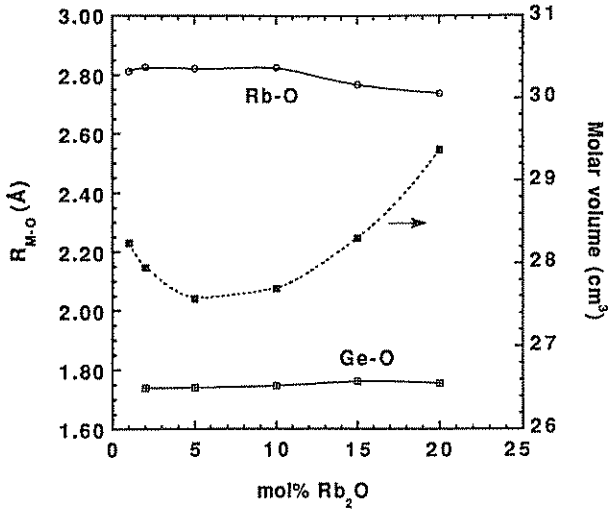

Fig. 3. Variation of the molar volume and Rb–O, Ge–O bond distances as a function of mol% Rb_2O in $xRb_2O\cdot(1-x)GeO_2$ glass series.

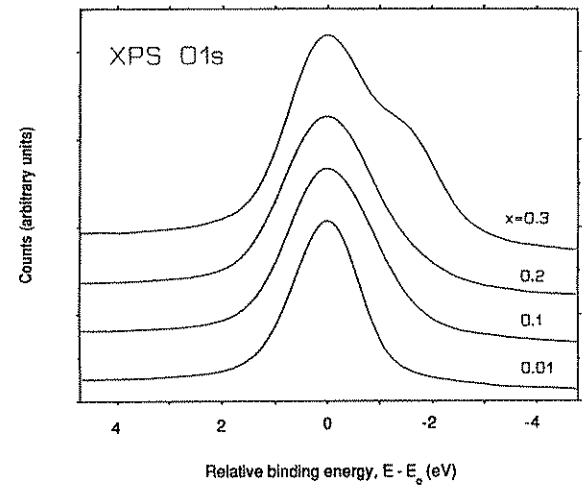

Fig. 4. O 1s XPS spectra of $xRb_2O\cdot(1-x)GeO_2$ glasses with binding energy scale relative to the binding energy of respective BOs (E_0) given in Table 5 (shoulder at relatively lower binding energy represents NBOs).

charge density between an NBO and a BO is reflected in the energy difference of corresponding peaks shown in Fig. 4. The area under the deconvoluted components represents the relative amount of the two types of oxygen and thus gives the fraction of NBO which is plotted as a function of Rb_2O concentration in Fig. 6. For comparison the NBO concentration for an alkali silicate system is also shown. Note that the NBOs in germanate glasses are far fewer than in corresponding silicates [10]. Also an appreciable amount of NBOs exists at the lowest Rb_2O concentration investigated (5 mol%).

Following the literature [31], we assume that the addition of Rb_2O to GeO_2 causes either the production of NBO or conversion of GeO_4 to GeO_6, and calculate the fraction of six-coordinated Ge, N_6,

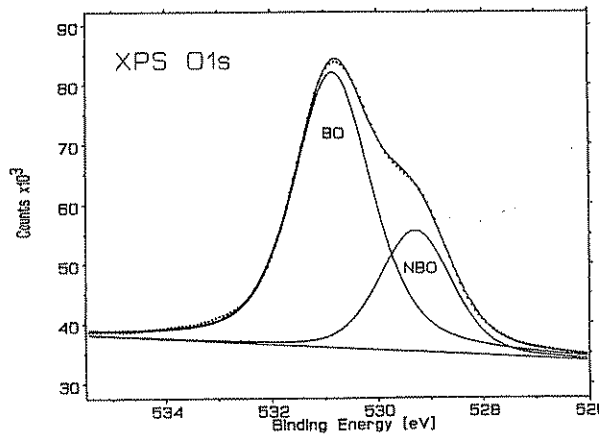

Fig. 5. Deconvolution of O 1s XPS spectrum of $0.3Rb_2O\cdot0.7GeO_2$ glass into the BO and NBO components.

Table 5
XPS results of O 1s parameters for the $xRb_2O\cdot(1-x)GeO_2$ rubidium germanate glasses

x	Peak energy (eV)		FWHM (eV)		A_{NBO}/A_{NBO+BO} (%)	N_6 (%)
	BO (E_0)	NBO	BO	NBO		
0.05	534.0	532.1	1.81	1.55	2.8	2.4
0.10	534.4	532.3	1.95	1.75	3.8	7.1
0.15	535.0	533.2	1.93	1.67	5.2	12.0
0.20	533.8	532.0	1.98	1.45	5.4	18.9
0.30	529.8	528.2	1.71	1.30	24.3	13.4
0.40	531.8	530.1	1.43	1.37	43.9	8.1

N_6 is calculated from the experimental fraction of NBO, A_{NBO}/A_{NBO+BO} (A is the area under the peak). E_0 is the binding energy of respective BO peaks.

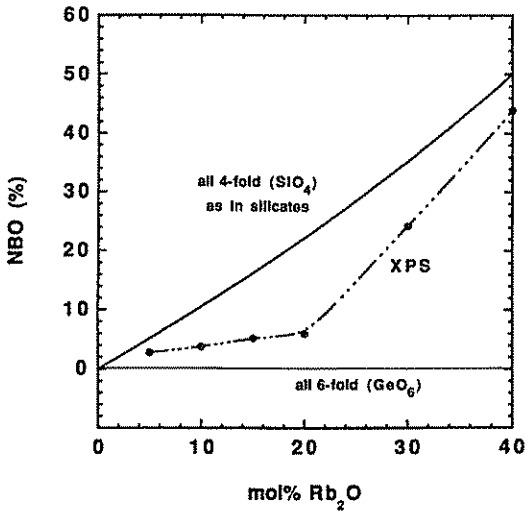

Fig. 6. The fraction of NBO determined from O 1s XPS of $x\mathrm{Rb_2O}\cdot(1-x)\mathrm{GeO_2}$ glasses. The solid lines show NBO fraction in silicate glasses comprising of only SiO_4 units and in a hypothetical germanate in which GeO_4 units convert to GeO_6 without forming any NBOs.

from the fraction of NBO (see Table 5): fraction of NBO $= 2(x-p)/(2-x)$ and $N_6 = p/(1-x)$, where x is the value in $x\mathrm{Rb_2O}\cdot(1-x)\mathrm{GeO_2}$ and p is the fraction of $x\mathrm{Rb_2O}$ which causes the conversion of GeO_4 into GeO_6. Fig. 7 shows the results of this analysis where the solid line represents a hypothetical condition in which all the addition of Rb_2O converts GeO_4 into GeO_6 without producing any NBO, i.e., $N_6 = x/(1-x)$. EXAFS results for the fraction of GeO_6, N_6, calculated from the increase in Ge–O bond distance (as shown in Fig. 2) are also shown in this figure for comparison.

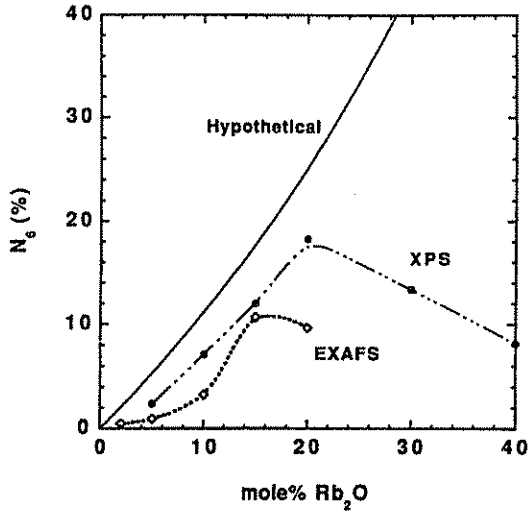

Fig. 7. The fraction of six-coordinated Ge, N_6, as a function of mol% Rb_2O in $x\mathrm{Rb_2O}\cdot(1-x)\mathrm{GeO_2}$ glass series. The solid line represents a hypothetical condition where no NBOs exist. The curves marked XPS and EXAFS are obtained from the analysis of O 1s XPS and Ge–O bond distance, respectively.

4. Discussion

4.1. $x\mathrm{Rb_2O}\cdot(1-x)\mathrm{GeO_2}$ glass series

The conversion of GeO_4 to GeO_6 structural units with the addition of alkali oxide in germanate glasses has been suggested from EXAFS [33], IR [34] and X-ray edge shift [35]. In the early studies of Ge EXAFS by Cox and McMillan [33], only the nearest neighbor oxygen shell could be observed. Their detailed analysis for lithium germanate glasses assumed the splitting of oxygen shell into two environments, with Ge–O distances ~ 1.71 and ~ 1.85 Å, respectively. The bond lengths of the two sites were found to be independent of the lithium content and were very close to 1.74 Å in fourfold α-quartz GeO_2 and 1.90 Å in sixfold rutile GeO_2. The CN from these two environments was used to calculate the ratio of GeO_6 to GeO_4. Although this might appear as direct evidence that the initial addition of alkali oxide simply converts GeO_4 to GeO_6 structural units, the error in CN around Ge is usually shown to be large, $\sim 30\%$ [30,32]. Further, the S/N (signal to noise) ratio for the larger Ge–O distance was too small to make reliable quantitative evaluation. Hence the fraction of GeO_6 from the CN estimation in this work is not definitive.

Very recently, Greaves and co-workers [36,37] established a fitting index method by constructing matrices for correlation between $\Delta\sigma^2$ and CN to calculate the back Fourier transform fitting error. In their best fit data of 95% accuracy, the precision of CN as well as $\Delta\sigma^2$ was $\sim \pm 10\%$. This accuracy is also the best value of precision in CN and $\Delta\sigma^2$ ever reported [31]. Now let us consider the possible variation of CN in our samples. The maximum value of N_6 from XPS is $\sim 20\%$ at 20 mol% Rb_2O, so that the corresponding maximum average CN of Ge is equal to $6\times 20\% + 4\times 80\% = 4.4$. Thus the variation of CN with Rb_2O mol% ranges only from 4 to

4.4. This variation of CN $\leq 10\%$ is too small to be extracted from EXAFS analysis which has an error of $\pm 10\%$ or higher. In other words, CN obtained from the EXAFS analysis is not accurate enough for monitoring the change in coordination of Ge in our germanate glasses.

In subsequent Ge EXAFS studies [34,38] on Li, Na and K germanate glasses, no evidence is given for the presence of the Ge–O peak at ~ 1.90 Å. Then the average measured Ge–O bond length has been used to determine the fraction of GeO_6. Here the observed increase of Ge–O distance with increasing alkali content is ascribed to the presence of GeO_6 structural units; it is assumed to be linearly dependent on the conversion of GeO_4 to GeO_6. Hence the increase of the Ge–O bond length is indirectly used to calculate N_6. Fig. 7 shows for the $x Rb_2O \cdot (1-x)GeO_2$ series that N_6 calculated from the Ge–O bond lengths is consistently smaller than that determined from XPS measurement of NBOs. Fig. 6.8 of the review article by Gurman [31] also shows large scattering of N_6 datapoints especially when the alkali concentration is high, indicating the uncertainty of estimating N_6 from EXAFS.

The determination of the NBO concentration from XPS has been proven to be precise in silicate glasses [10], and we may expect similar precision for the determination of NBOs in germanates. It is also reasonable that the charge compensation for alkali ions is provided either by the conversion of BO to NBO or that of GeO_4 to GeO_6 units. Then the determination of N_6 such as in Fig. 7 should be more precise from XPS than from EXAFS data. The XPS results indicate that at low Rb_2O concentration the major contribution of Rb_2O in germanate glasses is to convert GeO_4 to GeO_6 although some NBOs are also observable even at the lowest concentration of Rb_2O. However, as the concentration of Rb_2O increases beyond 15 mol%, N_6 from the XPS data starts to deviate from the solid curve and goes through a maximum at ~ 20 mol% Rb_2O. With further increase of Rb_2O, in fact, the fraction of six-coordinated Ge decreases. This decrease implies that the conversion of GeO_4 to GeO_6 gradually decreases and, instead, comparatively more NBOs are produced when Rb_2O is > 20 mol%. Now, because GeO_6 is a more compact packing of atoms than GeO_4, one would intuitively think that like N_6 the compactness of the Ge–O network would also vary with a maximum at ~ 20 mol% Rb_2O concentration. However the molar volume, V_m, shown in Fig. 3 does not exactly follow this prediction. Instead, its minimum value, and thus the maximum compactness, occurs at ~ 7 mol% rather than 20 mol% Rb_2O. The reason for this discrepancy is that the structural changes are more complicated than previously suggested [33–35,38]. It is true that GeO_4 units are converted to GeO_6 units with the addition of Rb_2O (Fig. 7) but that is not the only change. Fig. 6 shows that NBOs are also produced at the same time, although in smaller concentration than in silicates. Even with the initial addition of Rb_2O, both the GeO_6 units and the NBOs are produced in the structure. As we know, generally the occurrence of NBO upon the addition of alkali oxide leads to a loosening of the glass structure [8,39], which is opposite to the effect of forming GeO_6. So the maximum compactness would occur at an Rb_2O concentration which is less than the observed concentration of the N_6 maximum at 20 mol%.

Next, we ask how the molar volume correlates with the short-range local structure? Since the Rb–O distance remains the same to 10 mol% Rb_2O and decreases only a little thereafter (Table 2), it cannot account for the observed behaviour of V_m. The average local volume around Ge (i.e. the Ge–O distance) increases with increasing Rb_2O by a very small amount (Table 1), and its variation with mol% Rb_2O does not correlate at all with that of molar volume (see Fig. 3). If we examine the variation of molar volume and bond distances, we observe that the change in molar volume does not correlate with the Rb–O and Ge–O interatomic distances. Then it is possible that the observed variation of molar volume depends more on the CN of network-forming atoms, namely Ge and oxygen, rather than on the various interatomic distances. A comparison of Figs. 3 and 7 shows that the variation of CN around Ge with composition does not correlate with that of the molar volume.

From Rb EXAFS we determined second shell Rb–Ge distance (Table 3), which shows little variation with Rb concentration in comparison with the Rb–O and Ge–O distances. That is, it also shows no correlation with the concentration dependence of the molar volume. At the same time, one would expect

the second shell distances to be more representative of molar volume than the single shell distances. A possible explanation for the lack of correlation between V_m and the Rb–O, Ge–O or Rb–Ge distances is that a part of the molar volume is 'unoccupied' in the structure which is not affected by the various bond distances. The change in molar volume is mainly from the variation in 'unoccupied volume'. One can conceive that the unoccupied volume is the preferred pathway for diffusion of alkali atoms in glasses. Further experiments and analysis of data are needed to establish the validity of this suggestion.

The concept of MRN structure originated from the observation that the disorder around alkali ions in silicates is primarily of thermal origin [12,13]. The magnitude of disorder around Rb in our germanate glasses is almost an order of magnitude larger than that of alkali atoms in silicates (Table 2). We do not exactly know the contribution of thermal disorder to the observed disorder, yet we can say from a preliminary measurement at liquid helium temperature that the structural disorder around Rb is significantly more than that for the alkalis in silicates. It then follows that Rb is far more randomly distributed in a germanate glass than, for example, sodium in a silicate glass. Consequently the segregated channeled structure assumed for alkali migration in MRN is less meaningful for our case. We do not see any trivial effect of this difference on the variation of properties dependent on ion movement. Meanwhile, the increase in $\Delta\sigma^2_{Rb-O}$ with reduction of Rb_2O content (see Table 2) implies that the Rb environment is less uniform at low concentration. When more Rb_2O is added, the non-uniformity is averaged out and the environment around Rb becomes more homogeneous, resulting in smaller mean square displacement.

4.2. $0.2[yAg \cdot (1-y)Rb]_2O \cdot 0.8GeO_2$ mixed mobile ion glass series

The results of Ge EXAFS in Table 1 indicate that the Ge–O distance decreases as Rb is replaced by Ag, which is also the trend when the Rb_2O concentration is decreased in the binary $xRb_2O \cdot (1-x)GeO_2$ germanate system. From Rb EXAFS we note that the Rb–O distance increases as Rb is replaced by Ag, i.e., as y varies from 0 to 1 (Table 2). Again, the same is also expected as x decreases in the binary samples. Therefore, it appears that the substitution of Ag for Rb produces the same changes in structure as the reduction of Rb does in the binary $xRb_2O \cdot (1-x)GeO_2$ system. That is, the presence of Ag has little effect on the structure around Ge and Rb. This trend also appears to be true for the disorder around these two species. We suggest that Ag, being a highly deformable atom, accommodates the influence of composition variation and allows the local environment of more rigid alkali and network–former atoms to remain unaffected.

Our mixed Rb–Ag germanate glass series shows the typical mixed mobile ion effect, in that ionic conductivity, σ, has a minimum and its activation energy, E, has a maximum as Rb is replaced by Ag [22]. However, Ge–O and Rb–O distances and structural disorder, $\Delta\sigma^2$, vary monotonically with the same composition variation (Tables 1 and 2). The fundamental manifestation of the MMI effect is that the diffusivity of a mobile ion (e.g., Rb) decreases but monotonically as it is gradually substituted by another mobile ion (e.g., Ag) [40]; the effect is similar for both the ions. Then it is difficult to understand how the monotonic variation of Ge–O or randomness around Ge can account for the MMI in this system. Only those structural parameters can be important which involve the mobile ions. Further, for a structural feature to correlate with the MMI effect, it must vary in a complementary manner as diffusivity does when one cation is replaced by the other [40,41]. That is, we may expect the mobile ion–oxygen distance to be important for MMI if the increase of R_{Rb-O} with decreasing Rb fraction is accompanied by an increase of Ag–O distance with decreasing Ag fraction. Similarly, the disorder around a mobile ion could be relevant for MMI if the increase of $\Delta\sigma^2_{Rb-O}$ with decreasing Rb is matched by an increase of $\Delta\sigma^2_{Ag-O}$ with decreasing Ag. However, the Ag K-edge EXAFS results in Table 4 show that the Ag–O distance, the disorder and CN around Ag decrease significantly with decreasing Ag_2O content. These relatively larger changes in structural parameters for Ag than for Rb are expected from the large polarizability of Ag ions. The important observation is that the trend of the Ag–O distance is qualitatively opposite to that of the Rb–O distance as the two ions replace each other. The

same is true for disorder around Ag and Rb, respectively. Thus, the mobile cation–oxygen distance and the disorder around the mobile cation should not be the key to MMI effect in the present glass system.

From Table 4, it is not clear whether the structural change around Ag atom (namely, the increased Ag–O distance and $\Delta\sigma^2_{Ag-O}$ with increasing Ag/Rb ratio) is due to the replacement of Rb by Ag or only due to the increase of Ag concentration itself. To answer this question, one must conduct EXAFS experiment for the local structure around Ag atom in $zAg_2O \cdot (1-z)GeO_2$ binary germanate glass series. Without this information it is difficult to assess whether or not each of the mobile cations (Rb, Ag) stays in its own environment irrespective of Ag/Rb ratio. This assumption is important in a recent theory of MMI effect proposed by Maass et al. [42], which also considers that there are preferred sites for each type of cation. In fact, we have performed preliminary EXAFS experiments on the $zAg_2O \cdot (1-z)GeO_2$ series with $z = 0.02$, 0.05. 0.1, 0.15 and 0.2. The results indicate nearly the same Ge Fourier EXAFS spectra for all z values. That is, the Ge–O bond distance and structural disorder around the Ge atom remain almost unchanged. From Ag EXAFS, we note that the Ag–O distance also does not seem to change much. Unfortunately the signal-to-noise ratio for Ag EXAFS is not good and there may be interference from the Ag–Ag correlation presumably coming from Ag microprecipitates. To obtain more accurate structural information it will be necessary to repeat these experiments after eliminating the problem of Ag precipitation.

5. Summary

The presence of GeO_6 structural units besides tetrahedral GeO_4 units in a $xRb_2O \cdot (1-x)GeO_2$ glass series is supported by the increase of the Ge–O bond distance obtained from Ge EXAFS. However, quantitative evaluation of N_6 from XPS shows that the addition of Rb_2O introduces GeO_6 as well as NBOs as charge-compensating centers for Rb^+ for all $x \leq 0.2$. For $x > 0.2$, the concentration of NBOs increases at the expense of GeO_6. The variation of molar volume with composition does not correlate with that of various interatomic distances. We suggest the existence of an 'unoccupied volume' in the structure. The relatively large disorder around Rb in germanate glass indicates that the MRN model is less applicable to alkali germanate than to alkali silicate glasses.

The presence of Ag seems to have little effect on the local structure around Rb and Ge atoms in mixed $0.2[yAg \cdot (1-y)Rb]_20 \cdot 0.8GeO_2$ glasses. Replacement of Rb by Ag in mixed germanate glasses has the same effect on the Rb–O distance and disorder around Rb as the reduction of the Rb content in Rb germanate glasses. The Ag–O distance and disorder around Ag show a trend opposite to that of the Rb–O distance and disorder around Rb when Ag and Rb replace each other. Therefore, the mobile cation–oxygen distances and structural disorder around them should not be an important component of the MMI effect.

The authors wish to thank Dr A.R. Miller for his help with the XPS experiments. This work was supported by the Basic Energy Sciences Division of US Department of Energy under grant No. DE-FG02-90ER45419.

References

[1] K. Nassau, D.L. Chadwick and A.E. Miller, J. Non-Cryst. Solids 93 (1987) 115.
[2] D.L. Wood, K. Nassau and D.L. Chadwick, Appl. Opt. 21 (1982) 4276.
[3] P.P. Lottici, I. Manzini, G. Antonioli, G. Gnappi and A. Montenero, J. Non-Cryst. Solids 159 (1993) 173.
[4] A.O. Ivanov and K.S. Estrop'ev, Dokl. Akad. Nauk. USSR 145 (1962) 797.
[5] J.N. Mundy and G.L. Jin, Solid St. Ionics 24 (1987) 263.
[6] A. Margaryan and M.A. Piliavin, Germanate Glasses: Structure, Spectroscopy, and Properties, (Artech House, Norwood, MA, 1993) pp. 53–81.
[7] W.Vogel, Chemistry of Glass, transl. N. Kreidl (American Ceramic Society, Columbus, OH, 1985) p. 143.
[8] W.J. Zachariasen, J. Am. Ceram. Soc. 54 (1932) 3841.
[9] R. Brückner, H.-U. Chun and H. Goretzki, Glastech. Ber. 51 (1) (1978) 7.
[10] D.S. Goldman, Phys. Chem. Glasses 27 (3) (1986) 128.
[11] G.S. Henderson and M.E. Fleet, J. Non-Cryst. Solids 134 (1991) 259.
[12] G.N. Greaves, A. Fontaine, P. Lagarde, D. Raoux and S.J. Gurman, Nature 293 (1981) 611.
[13] G.N. Greaves, J. Non-Cryst. Solids 71 (1985) 203.
[14] G.N. Greaves and K.L. Ngai, in: Defects in Insulating Materials, ed. O. Kanert and J.M. Spaeth (World Scientific, Singapore, 1993) p. 53.

[15] C. Huang and A.N. Cormack, J. Chem. Phys. 93 (1990) 8180.
[16] B. Vessal, G.N. Greaves, P.T. Marten, A.V. Chadwick, R. Mole and S. Houde-Walter, Nature 356 (1992) 504.
[17] H. Melman and S.H. Garofalini, J. Non-Cryst. Solids 134 (1991) 107.
[18] B.M.J. Smets and T.P.A. Lommen, J. Non-Cryst. Solids 46 (1981) 21.
[19] D.E. Day, J. Non-Cryst. Solids 21 (1976) 343.
[20] E.I. Kamitsos, A.P. Patsis and G.D. Chryssikos, in: Physics of Non-Crystalline Solids, ed. L.D. Pye, W.C. LaCourse and H.J. Steven, (Taylor and Francis, London, 1992) p. 460.
[21] E.F. Riebling, J. Chem. Phys. 35 (1971) 804.
[22] W.C. Huang and H. Jain, to be published.
[23] M.A. Marcus and W. Flood, Rev. Sci. Instrum. 62 (1991) 839.
[24] S.M. Heald, in: X-ray Absorption: Principles, Applications, Techniques of EXAFS, SEXAFS and XANES, ed. D.C. Koningsberger and R. Prins (Wiley, New York, 1988) p. 119.
[25] D.C. Koningsberger, in: X-ray Absorption: Principles, Applications, Techniques of EXAFS, SEXAFS and XANES, ed. D.C. Koningsberger and R. Prins (Wiley, New York, 1988) p. 163.
[26] P.A. Lee, P.H. Citrin, P. Eisenberger and B.M. Kincaid, Rev. Mod. Phys. 53 (1981) 769.
[27] B. Rupp, B. Smith and J. Wong, Comput. Phys. Commun. 67 (1992) 543.
[28] J.J. Rehr, J. Mustre de Leon, S.I. Zabinsky and R.C. Albers, J. Am. Chem. Soc. 113 (1991) 5135.
[29] D.A. Shirley, Phys. Rev. B5 (1972) 4709.
[30] B.K. Teo, EXAFS: Basic Principles and Data Analysis (Springer, Berlin, 1986).
[31] S.J. Gurman, in: Applications of Synchrotron Radiation, ed. C.R.A. Catlow and G.N. Greaves (Blackie, Glasgow, 1990) p. 140.
[32] D.E. Sayers and B.A. Bunker, in: X-ray Absorption: Principles, Applications, Techniques of EXAFS, SEXAFS and XANES, ed. D.C. Koningsberger and R. Prins (Wiley, New York, 1988) p. 211.
[33] A.D. Cox and P.W. McMillan, J. Non-Cryst. Solids 44 (1981) 257.
[34] S. Sakka and K. Kamiya, J. Non-Cryst. Solids 49 (1982) 103.
[35] C.D. Yin, K. Morikawa, F. Marumo, Y. Gohshi, Y.Z. Bai and S. Fukashima, J. Non-Cryst. Solids 69 (1984) 97.
[36] G.N. Greaves, A.J. Dent, B.R. Dobson, S. Kalbitzer, S. Pizzini and G. Muller, Phys. Rev. B45 (1992) 6517.
[37] S.N. Houde-Walter, J.M. Inman, A.J. Dent and G.N. Greaves, J. Phys. Chem. 97 (1993) 9330.
[38] C. Lapeyre, J. Petiau and G. Calas, in: The Structure of Non-Crystalline Materials, ed. P.H. Gaskell, J.M. Parker and E.M. Davis (Taylor and Francis, London, 1983) p. 42.
[39] B.E. Warren, Z. Kristallogr. Mineralogy Petrogr. 86 (1933) 349.
[40] H. Jain, N.L. Peterson and H.L. Downing, J. Non-Cryst. Solids 55 (1983) 293.
[41] H.L. Downing, N.L. Peterson and H. Jain, J. Non-Cryst. Solids 50 (1982) 203.
[42] P. Maass, A. Bunde and M.D. Ingram, Phys. Rev. Lett. 68 (1992) 3064.